ELECTRONIC SPECKLE PATTERN INTERFEROMETRY

A speckle pattern is a complicated interference phenomenon that is observed in two main areas of research: laser optics and stellar astronomy. In the case of lasers, speckle patterns are generated when the coherent light from the laser is reflected off an abraded or optically rough surface. The grainy or speckled appearance of the laser light when viewed after reflection is known as "laser speckle." In astronomy, it has been known for some time that highly magnified short-exposure images of stars have a similar speckled appearance when viewed through the atmosphere, and that each bright speckle has a size that is easily related to the diameter of the telescope. Figure 1 shows an example of both a laser speckle pattern and a stellar speckle pattern. The study of both kinds of patterns, with the aid of electronic imaging devices, is known as electronic speckle pattern interferometry. Laser speckle interferometry is a tool used in many areas of engineering for precise measurement of physical systems, whereas in astronomy, it is a way to compensate for the blurring of images caused by the atmosphere and to reconstruct extremely high-resolution images of astronomical objects.

Though they differ in some important ways, the two types of speckle patterns have a common origin. Light emanating from a laser is coherent, which means that it travels in phase in the form of a plane wave. After reflection from an abraded surface, however, the light is no longer coherent. Each point in the beam may be thought to have a random phase, and when brought into focus, the random phases interfere with one another, creating a field of speckles on the image plane. Likewise, if light from a distant star were monochromatic, it would arrive as a plane wave at the top of the earth's atmosphere. (To approximate the monochromatic situation, stars may be observed through a narrow wavelength band pass filter.) As the light travels down through the atmosphere to the telescope, it encounters inhomogeneities in the refractive index of the air, so that when the light enters the primary telescope aperture, random phase delays are again present. After brought to a focus by the telescope optics, the phase delays interfere, again creating a speckle pattern.

LASER SPECKLE INTERFEROMETRY

While laser speckle had been observed since the first use of lasers in the 1960s, the science of speckle interferometry began with the idea that the speckle fields could be used to make sensitive measurements of test samples, such as vibra-

tion or displacement studies (1). The extraction of information from the test sample is nondestructive and does not require that the sample have a specular surface. For these reasons, speckle interferometry has found many uses in engineering today.

Figure 2 shows a simple laser speckle interferometer system that uses a single laser as the light source. Collimated, coherent light from the laser strikes a beam splitter and then the double beam proceeds to the two "arms" of the interferometer, marked A and B in the figure. At the end of arm A are two mirrors, reflecting the light toward the imaging detector as a reference beam. At the end of arm B is a test sample with an optically rough surface. Light is reflected back to the beam splitter where it is recombined with light from arm A and imaged onto the imaging device. Images, like the one shown in Fig. 1(a), are then recorded by the imaging detector and transferred to computer.

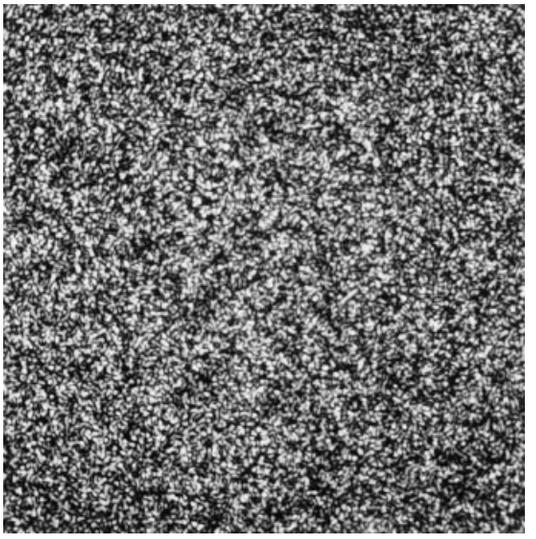

(a)

(b)

Figure 1. (a) Model speckle pattern that might be generated from a laser speckle interferometer, (b) model speckle pattern that might be generated by a star observed with a large telescope.

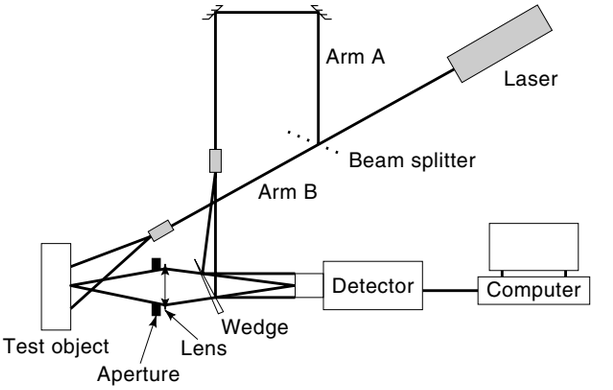

Figure 2. A simple laser speckle interferometry system.

In principle, many types of imaging devices could be used in a speckle interferometer. However, television camera systems (also known as vidicons) have typically been used in the past, and now charge-coupled device (CCD) cameras are common. These are relatively inexpensive and adequate for many laser speckle applications, in contrast to astronomical speckle interferometry systems, where the requirements for the imaging detector are much more stringent because of the intrinsic faintness of most target stars and the fast, random fluctuations of astronomical speckle patterns. (These fluctuations usually change faster than the standard video rate of 30 Hz.) Vidicons and CCDs also can interface easily with computers, so that digital images of the speckle patterns can be stored directly on computer for processing in various ways that enhance the contrast of the interference features. These and other imaging detectors are discussed in more detail in a later section.

Basic Characteristics of Laser Speckle Fields

The size of speckles in the speckle field is determined by the optical design of the interferometer. When a lens is used, as in Fig. 2, the speckles at the focal plane of the imaging device are referred to as "subjective speckles," since their size is determined in part by the magnification of the lens or lens system. Assuming that the lens images the surface of the object under study, the size of speckles σ at the imaging device is given by

$$\sigma \approx 1.2(1+M)\lambda F \tag{1}$$

where M is the magnification of the lens, F is its f/number and λ is the wavelength of light being used. This can be related to the size of speckles on the surface of the object, Σ, by

$$\sum \approx 1.2(1+M)\lambda F/M = \sigma/M \tag{2}$$

If the light reflected from the surface of the object is combined with a uniform, coherent reference beam, which is a very common technique in laser speckle interferometry, the size of speckles will change. This is becuse the image formed at the focal plane of the detector may be thought of as the sum of the interference patterns generated by pairs of points in the aperture. Each such pair would produce a series of fringes whose spacing is determined by the distance between the two

point-apertures (as in Michelson interferometry), but taken together, the various fringes form the complicated interference pattern of the speckle field. Without the reference beam, the size of the speckles is essentially determined by interference between light traveling through opposite sides of the lens, since pairs of points with the largest separation will have the smallest spacing between fringes. It is the diameter of the lens that therefore controls the speckle diameter in this case. Adding the reference beam has the effect of placing a strong central ray in the aperture, and then the most obvious interference effect generated by pairs of points is when one of the points is the central ray. The largest effective separation is then between the center of the aperture and the edge, which corresponds to a fringe spacing double that of the previous case, and the speckle size doubles likewise.

The distribution of brightness of the speckle field is another basic property of speckle patterns. Assuming that the test surface truly randomizes the phases from the incoming coherent laser light, and that many scattering points contribute to the image of the speckle field at the detector, it can be shown that the intensity distribution of a single speckle field follows the negative exponential distribution

$$p(I) = \frac{1}{I_0} \exp\left(\frac{-I}{I_0}\right) \tag{3}$$

where I is the intensity, $p(I)$ is the probability of a point in the image having intensity I, and I_0 is the average intensity of the field. It is interesting that in this case the most probable intensity at any point in the image is zero, since $p(I)$ is a monotonically decreasing function of I.

As with the size of speckles, the intensity distribution of speckles changes when a reference beam is introduced. In the case where the reference beam has intensity equal to the average intensity of the speckle field, the distribution becomes

$$p(I) = \frac{2}{I_0} \exp\left[-\left(1 + \frac{2I}{I_0}\right)\right] J_0(2\sqrt{2I/I_0}) \tag{4}$$

where J_0 is the zero-order Bessel function of imaginary argument. Again the most probable intensity is zero, and in practice the two distributions are difficult to distinguish visually. However, if the pattern is recorded electronically, its statistics can be derived easily.

A third important feature of laser speckle fields is the contrast C defined by

$$C = \sigma_I / I_0 \tag{5}$$

where σ_I is the standard deviation of intensity values (the noise) in the speckle field and I_0 is the average intensity of the field. In the case of an interferometer with a specular reference beam, as in Fig. 2, it can be shown that $C = \sqrt{2}$, but in many cases C is a constant that depends on details of the optical system (2). This means that the noise in a speckle pattern is proportional to the local average intensity, which is sometimes referred to as "multiplicative" intensity noise.

Two Common Methods of Speckle Correlation

While several important methods have been used for correlating speckle fields, this discussion will be limited to two. In the first, the object under analysis is placed in the interferometer and a speckle pattern is recorded. The sample is then subjected to whatever test the operator desires, and then a new speckle pattern is recorded of the same region of the sample. The two patterns can then be combined electronically by taking the negative of the first pattern and adding it to the second. If the two patterns are identical, which is to say that the two images are perfectly correlated, then the speckles will exactly cancel and the result will obviously be zero. If the two patterns are uncorrelated in some regions of the speckle field, then the speckles will not cancel and the sum at a given speckle location will vary from zero in a random fashion in these regions. This can give rise to a speckled fringe pattern, where fringes contour lines of equal displacement in the sample.

An example of a speckled fringe pattern is shown in Fig. 3. This image was formed as a result of the above analysis when the model sample experienced a shear in the direction perpendicular to the plane of the sample surface between recording the first and second speckle patterns. The displacement of the sample was linear in the vertical direction, creating a fringe pattern following the contours of equal displacement in the horizontal direction. A dark fringe occurs when the displacement is equal to a multiple of the wavelength of the laser light. The technique described here is a powerful tool in strain analysis of mechanical pieces, allowing for measure of minute warping or shearing effects, but the contrast in the fringes is often poor.

A second kind of correlation technique involves displacing speckle images slightly from one another. As in the previous technique, one exposure is typically recorded before some mechanical test and a second after it is complete. The images are displaced slightly by a row or column shift of the first digital image and then added together. If the two images are highly correlated, there will be speckle pairs or "doublets" all over the field separated by the shift given the first image. If the fields are not correlated, the doublets will not be present. The occurrence of speckle doublets is easy to determine either

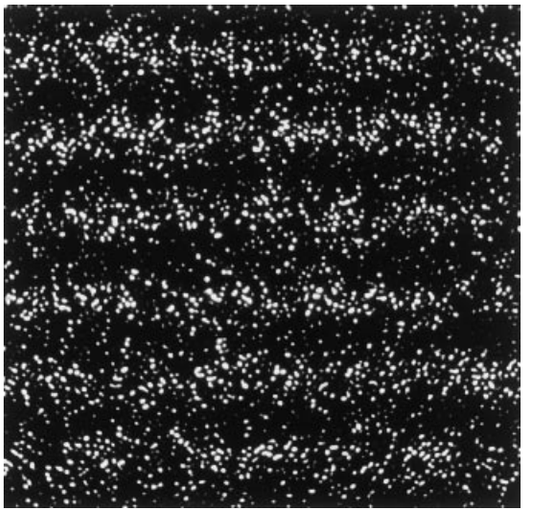

Figure 3. A model speckled fringe pattern, as generated in a displacement analysis.

by spatial filtering or by computing the spatial frequency power spectrum of the summed image, $Q(\boldsymbol{u})$, given by

$$Q(\boldsymbol{u}) = \left| \int I(\boldsymbol{x}) e^{-2\pi j \boldsymbol{x}\cdot\boldsymbol{u}} \right|^2 \tag{6}$$

where $I(\boldsymbol{x})$ is the summed image, $\boldsymbol{x}$ is the variable describing position on the image plane, and $\boldsymbol{u}$ is the spatial frequency variable conjugate to $\boldsymbol{x}$. The fringe pattern formed in this way tends to have very high contrast, and fringes only form if the two fields are highly correlated.

Both correlation techniques described here were first used not with electronic detectors but with speckle interferometry done with photographic plates, or "speckle photography." Each speckle pattern image had to be developed and studied later. Electronic detectors made possible real-time fringe pattern processing, which not only made the speckle experiments faster, but also made larger the number of correlation techniques that could be easily implemented.

Motion and Vibration Analysis

Two of the simplest kinds of speckle analyses can be done by visual inspection of the recorded speckle patterns. The first is motion. If a test sample is slowly moving in the speckle interferometer, the speckle pattern it generates at the imaging detector will change. The speckles will begin to twinkle, since the intensity of individual speckles is very sensitive to the position of the sample. This type of analysis is often used to monitor holographic recording, especially when the sample may expand during the recording process because of change in humidity or some other variable.

Vibration analysis is another example. If a sample is vibrating, and the amplitude of the vibrations is more than a fraction of a wavelength, the speckle pattern in the region of the vibration will begin to blur out and lose contrast as the speckles begin to change in intensity with the vibration. As a result, a speckle pattern recorded from a vibrating object will have a loss of contrast in regions that are moving. Nodal lines in the sample (areas of little or no motion) will still show the familiar high-contrast speckle pattern. In this way, speckle patterns can map the nodal structure of samples under vibration.

Displacement and Misalignment Analysis

Displacement of a test object can occur either in a direction in the plane of the surface of the object or in a direction perpendicular to the object surface (in the line of sight of the imaging system). For displacement in the line of sight of the imaging system, the previously described correlation techniques are often used. For localized displacement in the plane of the surface of the test object, several specialized types of speckle interferometers have been used and optimized for measure of in-plane displacement, such as the pioneering instrument of Leendertz (3). This instrument produced fringe patterns based on optical path length differences from two laser beams when the sample was moved. It is also true that small in-plane displacements of a test sample produce a speckle pattern that is merely shifted from the original pattern. This fact lends itself to a kind of double exposure analysis similar to the one described above. An exposure is taken before and after the test sample is shifted. These images are then summed. Speckle doublets will then be present in the summed exposure, where the spacing between the matching speckles scales with the physical displacement. Once the spatial frequency power spectrum of the image is formed, a fringe pattern will be present where the spacing of the fringes is inversely proportional to the physical displacement.

A misalignment, or tilt, in a physical system can also be measured with a speckle interferometer. It is possible to show that for laser light at normal incidence to the test surface, and viewing of the surface likewise near the normal, the test sample will act as a mirror under small rotations about any axis that lies in the plane of the surface of the sample. This means that if the sample is tilted by an amount $\delta\Phi$, the speckle pattern will be rotated through an angle $2 \cdot \delta\Phi$. At the image plane, this rotation of the speckle pattern will be viewed as a translation of the speckles. If the camera system is defocused by a known amount δU, and a double exposure speckle pattern is recorded before and after the tilt, the amount of tilt can be derived from the speckle displacement by

$$\delta\Phi = d/2M\,\delta U \tag{7}$$

where d is the displacement of the speckle pairs and M is the system magnification.

STELLAR SPECKLE INTERFEROMETRY

In conventional imaging with ground-based telescopes, astronomers must contend with the atmosphere, which blurs images significantly. The problem is so severe that for virtually all research class telescopes in operation today, the resolution of images is not determined by the optical design of the telescope but rather by the atmosphere through which the images are viewed. Loss of resolution is caused by a combination of two effects: first, inhomogeneities in the refractive index of the air above the telescope aperture break up stellar images and spread the light over a much broader region at the telescope focus than if the atmosphere were not present, and second, these inhomogeneities vary rapidly with time. Stellar speckle interferometry is a way to compensate for the blurring effects of the atmosphere and obtain very high-resolution information about astronomical objects from the ground. The method is usually performed on data taken at a large-aperture telescope, and high-resolution images are "reconstructed" after the observation. For this reason, it is referred to as a single-aperture passive technique, in contrast to other methods such as adaptive optics, where high-resolution images are built up during the observation, or Michelson interferometry, where more than one aperture is used to make observations. High-resolution images play a key role in several areas of astronomy. One of the most important areas is in deriving the orbits of binary stars. Binary star orbits are currently the only well-established way to obtain estimates of the masses of stars. High-resolution images also yield important information about the environment around young stars and the percentage of double and multiple star systems in young stellar associations. Speckle interferometry has made a significant contribution to several other kinds of astronomy, such as imaging asteroids and planets from the ground, measuring stellar diameters, and obtaining high-resolution information about supernova remnants.

Large Telescopes and the Atmosphere

In typical astronomical imaging applications the target is very faint, and a long exposure time is necessary to obtain a high-quality image. Over such long time scales, the effect of the atmosphere is such that a perfect source is blurred into a smooth quasi-Gaussian image with width ranging from a few tenths of a second of arc to several arcseconds, depending on observing conditions. It was first realized in the 1960s that highly magnified short exposure images of stars are not simply smooth quasi-Gaussian images, but instead are speckle patterns that have quasi-Gaussian envelope. The speckles form as a direct consequence of the effect of the atmosphere on the light coming from the star.

To see why this is so, consider an idealized astrophysical point source of monochromatic radiation. If this radiation were to enter the telescope in the absence of the atmosphere, it would be a plane wave and would therefore have uniform magnitude and phase across the telescope aperture. For the purposes of this discusison, it will be sufficient to use the model of a scalar electromagnetic field, so that the "aperture function" may be defined as the scalar (complex-valued) function representing the electromagnetic field entering the primary telescope aperture. An elementary theorem from optics states that the image of a perfect point source (known as the point spread function and henceforth called the PSF) of the telescope is the modulus square of the Fourier transform of the aperture function (4):

$$S(\boldsymbol{x}) = \left| \int A(\boldsymbol{z}) e^{-2\pi j \boldsymbol{x}\cdot\boldsymbol{z}/\lambda} \, d\boldsymbol{z} \right|^2 = |\hat{A}(\boldsymbol{x})|^2 \tag{8}$$

where $\boldsymbol{z}$ is the variable describing the plane of the aperture, $\boldsymbol{x}$ is the variable describing the image plane, $S(\boldsymbol{x})$ is the PSF, $A(\boldsymbol{z})$ is the aperture function, and $\hat{\ }$ denotes the Fourier transform. Figure 4 shows a sample zero atmosphere aperture function and PSF for a large telescope. The width of the PSF defines the resolution obtainable at the image plane. Since in astronomy the image corresponds to the intensity distribution projected on the sky (where the position of objects are measured in angular terms), it is common to refer to the width of the PSF in terms of arcseconds, as shown in Fig. 4(b).

The atmosphere changes the character of the aperture function. Because of motion and temperature fluctuations in the air above the telescope aperture, inhomogeneities in the refractive index develop. These inhomogeneities break the aperture into cells with a typical length scale of about 10 cm that are translated by a prevailing wind (in the simplest model) across the telescope aperture on a typical time scale of about 10 ms. Within a cell, the phase of the aperture function remains roughly uniform but it takes on different values from cell to cell. Because of the relationship between the aperture function and the PSF, the PSF is likewise changed; in fact, the time-evolution of the aperture function implies that the PSF is also time-dependent. If the atmosphere is frozen at a particular instant in time, the resulting PSF may be described as the sum of interference patterns between pairs of subapertures defined by the cells arising from the inhomogeneities in the refractive index. Just as with the size of laser speckles, each such pair would produce a fringe pattern whose spacing is determined by the distance between the two subapertures (as in Michelson interferometry), but taken to-

(a)

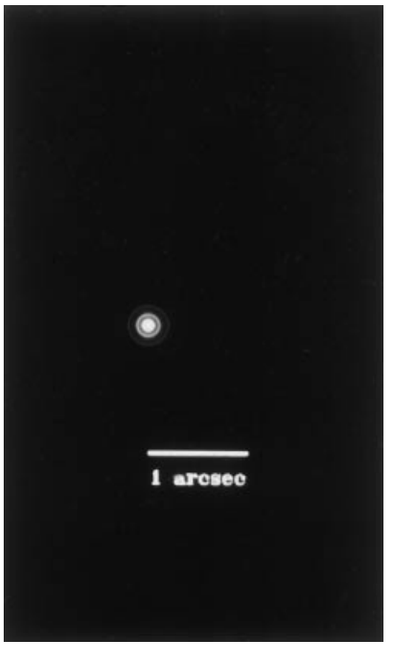

(b)

Figure 4. (a) Gray scale plot of the aperture function of a point source for a large telescope in the absence of the atmosphere. Since the aperture function is complex values, only the phase is plotted. The central region is assumed to be occulted by a secondary mirror. (b) The resulting point spread function from the aperture function in (a). Except for the occultation of the central region of the aperture, this would be the familiar Airy pattern from diffraction theory.

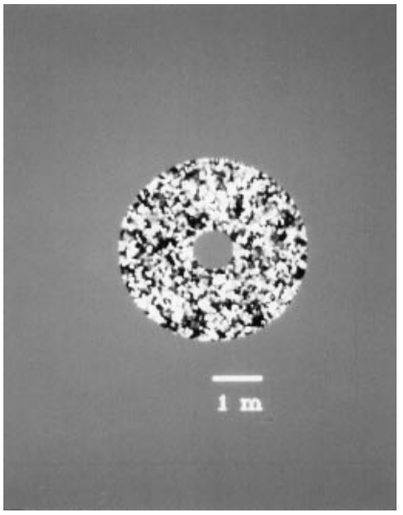

(a)

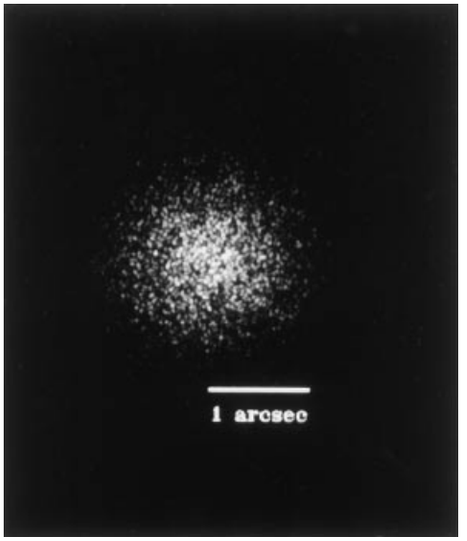

(b)

Figure 5. (a) Gray scale plot of a model instantaneous aperture function of a point source for a large telescope in the presence of atmospheric fluctuations. Since the aperture function is complex valued, only the phase is plotted. The central region is assumed to be occulted by a secondary mirror. (b) The resulting point spread function from the aperture function in (a), which is known as a stellar speckle pattern.

gether, the various fringe patterns form a speckle pattern. The speckles fill a broad region, typically 1 to 2 arcseconds in diameter on the image plane, but have a characteristic width similar to that of the diffraction-limited PSF of the telescope. An example of an (instantaneous) aperture function and PSF of a large telescope in the presence of atmospheric fluctuations is shown in Fig. 5. If Fig. 5 is now evolved in time, some of the phase cells pass out of the telescope aperture and new ones enter, and so the position and intensity of the speckles change on the image plane. On an exposure considerably longer than the time scale of atmospheric fluctuations, the speckle nature of the PSF washes out to leave only the shape of the broad quasi-Gaussian envelope, called the "seeing disk" of the star. For this reason, the resolution possible with conventional ground-based astronomy is much poorer than the diffraction-limited resolution of large telescopes. While the speckle patterns contain structure on the scale of the diffraction limit, these structures are lost in any exposure of an object longer than a few tens of milliseconds.

"Classical" Speckle Interferometry

The first technique for obtaining high-resolution information in the presence of atmospheric turbulence was developed by Labeyrie (5) in 1970. He pointed out that there is a way to obtain the diffraction-limited spatial frequency power spectrum of an object from a collection of individual speckle patterns. For sources of sufficient simplicity, such as binary stars, the power spectrum is a powerful tool for deducing high-resolution features. This was an important initial step toward high-resolution image reconstruction.

As mentioned above, the fluctuations of the atmosphere occur on a time scale of typically about 10 ms, so a stellar speckle observation would consist of a sequence of many short exposures of this typical exposure length. Each frame is then a fixed quasi–time-independent speckle pattern like the one shown in Fig. 5(b). In this case, each frame preserves structure on scales much smaller than the seeing disk, as evidenced by the speckles themselves and to the extent that the speckles can be resolved by the imaging detector on this time scale, each frame contains high angular resolution about the source.

Suppose that the object of interest is a binary star. Then the speckle patterns will exhibit speckle doublets at the vector separation of the two companions, as shown in Fig. 6. Of course, these speckle pairs will occur at various places on the

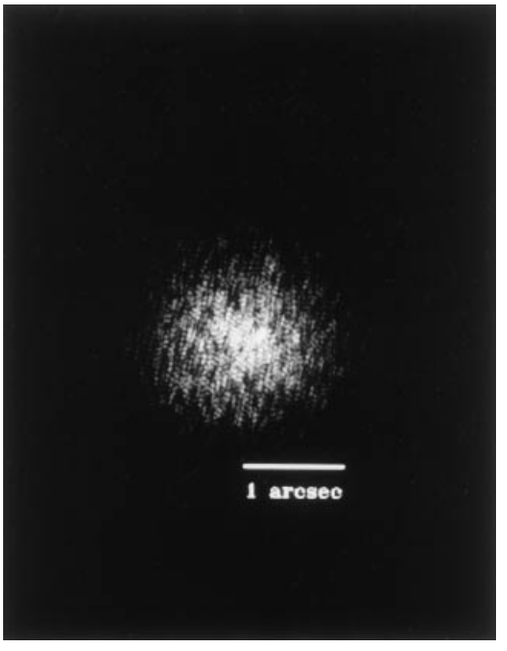

Figure 6. A model speckle pattern of a binary star, exhibiting double speckles. In this example, the separation vector of the two components is about twice the size of a speckle and directed toward 1 o'clock.

image plane, but they may be collected together by considering the autocorrelation function of the frame, which, up to a normalization factor, is equivalent to the histogram of the distance vectors between photon pairs. The autocorrelation function $\gamma(\boldsymbol{x})$ of a frame is defined by

$$\gamma(\boldsymbol{x}) = \int I^*(\boldsymbol{x}_1) I(\boldsymbol{x}_1 + \boldsymbol{x})\, d\boldsymbol{x}_1 \tag{9}$$

where $I(\boldsymbol{x})$ is the frame image and * denotes complex conjugate. The Fourier transform of the image autocorrelation is the image power spectrum (defined as the modulus square of the Fourier transform of the frame image). The frame image, on the other hand, is the convolution of the instantaneous point spread function $S(\boldsymbol{x})$ with the actual intensity distribution of the object $O(\boldsymbol{x})$, where the convolution integral is defined by

$$I(\boldsymbol{x}) = \int O(\boldsymbol{x}_1) \cdot S(\boldsymbol{x} - \boldsymbol{x}_1)\, d\boldsymbol{x}_1 \tag{10}$$

In the Fourier domain, a convolution becomes an ordinary product so that

$$\hat{I}(\boldsymbol{u}) = \hat{S}(\boldsymbol{u}) \cdot \hat{O}(\boldsymbol{u}) \tag{11}$$

where$\hat{}$ once again denotes the Fourier transform and the spatial frequency variable conjugate to $\boldsymbol{x}$ is $\boldsymbol{u}$. Taking the modulus square of this expression and averaging over many frames, the average image power spectrum is obtained:

$$\langle |\hat{I}(\boldsymbol{u})|^2 \rangle = \langle |\hat{S}(\boldsymbol{u})|^2 \rangle \cdot |\hat{O}(\boldsymbol{u})|^2 \tag{12}$$

where $\langle\ \rangle$ denotes the average over many frames. The function $\langle |\hat{S}(\boldsymbol{u})|^2 \rangle$ is known as the speckle transfer function. If a speckle observation is performed on the binary star, $\langle |\hat{I}(\boldsymbol{u})|^2 \rangle$ can be obtained by Fourier transforming the average autocorrelation of many frames of data. The same process on a point source (that is, an unresolved star) yields an estimate of $\langle |\hat{S}(\boldsymbol{u})|^2 \rangle$. As Eq. (12) shows, the true binary power spectrum can then be obtained by division, where such a division is valid in the region where $\langle |\hat{S}(\boldsymbol{u})|^2 \rangle$ is nonzero. In fact, the average point spread function power spectrum is nonzero out to the diffraction limit of the telescope, and the method works not only for binary stars but also for general objects. In the case of a binary system, the power spectrum is a fringe pattern. The spacing of the fringes is related to the separation of the stars, the orientation of the finges defines the relative orientation of the two stars (up to a 180° ambiguity), and the amplitude of the fringes is related to the relative brightness of the components. A variation on the autocorrelation method described here called the directed vector autocorrelation (6) can remove this ambiguity in the orientation, and is particularly useful in the study of binary stars.

The Speckle Transfer Function

As above, the speckle transfer function $T(\boldsymbol{u})$ is defined by

$$T(\boldsymbol{u}) = \langle |\hat{S}(\boldsymbol{u})|^2 \rangle \tag{13}$$

and relates the image power spectrum to the true object power spectrum. Theoretical models of $T(\boldsymbol{u})$ generally break the function into two components, a seeing-limited (low-frequency) portion approximated by

$$T_{\mathrm{lf}}(u) = |T_{\mathrm{t}}(u)|^2 \exp\left\{-6.88 \left(\frac{\lambda u}{r_0}\right)^{5/3} \left[1 - \left(\frac{\lambda u}{r_0}\right)^{1/3}\right]\right\} \tag{14}$$

and a diffraction-limited (high-frequency) portion approximated by

$$T_{\mathrm{hf}}(u) = 0.435 \left(\frac{r_0}{D}\right)^2 T_{\mathrm{t}}(u) \tag{15}$$

where $u \equiv |\boldsymbol{u}|$, r_0 is the "Fried parameter" describing the length scale of coherence cells in the aperture function, D is the telescope diameter, λ is the wavelength of observation, and $T_{\mathrm{t}}(u)$ is the (diffraction-limited) telescope transfer function. Though most of the power is in the low-frequency seeing-limited portion of the function due to the attenuation factor $(r_0/D)^2$ in the high-frequency portion, a nonzero high-frequency shoulder can also be seen out to the diffraction limit of the telescope. As discussed above, for a binary star, a fringe pattern would appear on top of the speckle shoulder, but more complicated objects would exhibit other functional forms in this region.

The low-frequency portion of the transfer function has a width that is determined by the Fried parameter. If r_0 is large, the seeing peak in frequency space is large, and the seeing disk on the image plane is therefore small, but if r_0 is small, then the low-frequency portion of the transfer function is small and the seeing disk is large. The quantity r_0/λ, which is a measure of the width of the low-frequency transfer function, is sometimes called the "seeing cutoff" in frequency space. The high-frequency portion of the transfer function is an attenuated version of the transfer function of the telescope, which means that the speckle transfer function manifestly extends to the diffraction-limit, roughly given by the ratio D/λ in the frequency plane. The attenuation factor involves the quantity $(r_0/D)^2$; because of the relationship between the Fried parameter and the seeing, the value of the transfer function on the speckle shoulder is therefore a sensitive function of the seeing.

An important consideration of the method of speckle interferometry is the expected signal-to-noise ratio (SNR) of the image power spectrum. In the high-frequency wing of the power spectrum (i.e., above the seeing cutoff), the SNR of a general object $O(\boldsymbol{x})$ is given by

$$\frac{S}{N}(\boldsymbol{u}) = \sqrt{M} \frac{n_{\mathrm{sp}} \cdot T_{\mathrm{t}}(\boldsymbol{u}) \cdot |\hat{O}(\boldsymbol{u})|^2}{1 + n_{\mathrm{sp}} \cdot T_{\mathrm{t}}(\boldsymbol{u}) \cdot |\hat{O}(\boldsymbol{u})|^2} \tag{16}$$

where n_{sp} is the number of photons per speckle, and M is the number of frames averaged. When the number of photons per speckle is small compared to $T_{\mathrm{t}}(\boldsymbol{u}) \cdot |\hat{O}(\boldsymbol{u})|^2$, the SNR increases linearly with n_{sp}, meaning essentially that the frames are limited by photon statistics, and when the number of photons per speckle is large compared to $T_{\mathrm{t}}(\boldsymbol{u}) \cdot |\hat{O}(\boldsymbol{u})|^2$, the SNR becomes asymptotically independent of n_{sp}, and the frames are limited by the atmospheric process.

This interplay between photon statistics and the atmosphere also determines the optimal frame exposure time. The frame time should be chosen so that the motion of the speck-

les within the frame is small, but if too short a frame time is chosen, frames will be photon-starved and this leads to a loss of SNR. On the other hand, if too long a frame time is chosen, speckle motion will lead to a loss of contrast in the frames, and again the SNR is reduced. It also depends on atmospheric (or equivalently, on seeing) conditions in the sense that shorter frame times are required when the seeing is poor.

Image Reconstruction

In principle, if one had a diffraction-limited estimate of the (generally complex-valued) function $\hat{O}(\boldsymbol{u})$, it would be simple to Fourier invert the function to obtain a reconstructed image. In order to do that, however, one needs to have estimate of both the modulus *and* the phase of $\hat{O}(\boldsymbol{u})$. Classical speckle interferometry as discussed above falls short of providing true image reconstructions because the recovered function is the object's power spectrum, that is, $|\hat{O}(\boldsymbol{u})|^2$, and clearly contains no phase information. This is known as the "phase problem" in speckle interferometry.

Solutions to the phase problem began to appear in the literature starting in the early 1970s. Some of the most common methods that have been used to reconstruct images from speckle data since that time include speckle location rearrangement, the Knox-Thompson algorithm, and bispectral analysis. The first method does not explicitly calculate the phase of the object's Fourier transform, but consists of a manipulation of the speckle patterns in the image plane that results in a high-resolution image. The last two methods do provide a means of calculating the phase of $\hat{O}(\boldsymbol{u})$, which is then combined with the modulus estimate, derived from the classical autocorrelation analysis.

Speckle Location Rearrangement. One approach to obtaining diffraction-limited images from speckle data is to consider bright, clearly identifiable speckles as estimates of the diffraction-limited PSF of the telescope. In general, speckle patterns contain speckles of varying brightness, and the fainter speckles are not clearly identified. For brighter objects, where many photons are detected in each frame, many speckles are clearly visible, as in Fig. 1(b), but for fainter objects, this may not be the case. Take, for example, the case where only the brightest speckle is easily identifiable in each frame. In this case, a simple way to proceed is to shift each frame so that the speckle is in the center of the frame (or the brightest pixel is in the center of the frame), and then co-add all of the frames. This is known as the "shift-and-add" technique (7).

A slightly more complicated approach is possible when there is sufficient contrast in each frame to identify several speckles (8). In this case, each frame of a general object may be written as

$$I(\boldsymbol{x}) = \left\{ \left[\sum_{\mathrm{i}=1}^{n} \delta(\boldsymbol{x}_{\mathrm{i}}) \right] * p(\boldsymbol{x}) \right\} * O(\boldsymbol{x}) \tag{17}$$

where n is the number of speckles identified in the frame, $\delta(\boldsymbol{x})$ is the impulse function, the $\boldsymbol{x}_{\mathrm{i}}$ represent the locations of the speckles on the frame, $p(\boldsymbol{x})$ is the profile of a single speckle, $I(\boldsymbol{x})$ and $O(\boldsymbol{x})$ are the frame image and the true object intensity distribution as previously defined, and $*$ denotes the convolution integral. The frame image can, for example, be iteratively deconvolved by the impulse field, leaving an image of $p(\boldsymbol{x}) * O(\boldsymbol{x})$. The function $p(\boldsymbol{x})$ can be obtained from a point source observation, and a further deconvolution can be performed to yield the desired function $O(\boldsymbol{x})$.

Knox–Thompson Algorithm. Knox and Thompson's solution (9) to the phase problem involves the analysis of a generalized version of the frame image power spectrum called the frame cross-spectrum, defined by

$$X(\boldsymbol{u}_1, \boldsymbol{u}_2) = \hat{I}(\boldsymbol{u}_1)\hat{I}^*(\boldsymbol{u}_2) \tag{18}$$

(The power spectrum is obtained when $\boldsymbol{u}_1 = \boldsymbol{u}_2$.) Using Eq. (11), this can be rewritten in terms of the instantaneous point spread function and the true object intensity distribution. Averaging over many frames results in

$$\langle X(\boldsymbol{u}_1, \boldsymbol{u}_2) \rangle = \langle \hat{S}(\boldsymbol{u}_1)\hat{S}^*(\boldsymbol{u}_2) \rangle \hat{O}(\boldsymbol{u}_1)\hat{O}^*(\boldsymbol{u}_2) \tag{19}$$

The function $\langle \hat{S}(\boldsymbol{u}_1)\ \hat{S}(\boldsymbol{u}_2) \rangle$ is known as the cross-spectral transfer function. It can be shown that the cross-spectral transfer function takes on nonnegligible values only for frequencies $\boldsymbol{u}_1$ and $\boldsymbol{u}_2$ satisfying

$$|\boldsymbol{u}_1 - \boldsymbol{u}_2| < \frac{r_0}{\lambda} \tag{20}$$

which is to say, their difference has to be smaller than the seeing cutoff in frequency space. Since this region is small compared to the region of the frequency plane inside the diffraction limit, it is convenient to define $\boldsymbol{u}_1 \equiv \boldsymbol{u}$ and $\boldsymbol{u}_2 \equiv \boldsymbol{u} + \Delta\boldsymbol{u}$, with $|\Delta\boldsymbol{u}| < r_0/\lambda$. Then the phase of Eq. (19) can be written in the form

$$\arg[\langle \hat{I}(\boldsymbol{u})\hat{I}^*(\boldsymbol{u} + \Delta\boldsymbol{u}) \rangle] = \phi_O(\boldsymbol{u}) - \phi_O(\boldsymbol{u} + \Delta\boldsymbol{u}) + \phi_{XT}(\boldsymbol{u}, \boldsymbol{u} + \Delta\boldsymbol{u}) \tag{21}$$

where ϕ_O is the phase of $\hat{O}$ and ϕ_{XT} is the phase of the cross-spectral transfer function. In analogy with classical speckle interferometry, the function $\phi_{XT}(\boldsymbol{u}, \boldsymbol{u} + \Delta\boldsymbol{u})$ can be measured using a point source calibration object, then subtracted from the phase of the image cross-spectrum. The result is

$$\arg\{[\hat{I}(\boldsymbol{u})\hat{I}^*(\boldsymbol{u} + \Delta\boldsymbol{u})]\} - \phi_{XT}(\boldsymbol{u}, \boldsymbol{u} + \Delta\boldsymbol{u}) = \phi_O(\boldsymbol{u}) - \phi_O(\boldsymbol{u} + \Delta\boldsymbol{u}) \tag{22}$$

which is a difference equation for the function ϕ_O. Using two nonparallel values for $\Delta\boldsymbol{u}$ and an appropriate initial condition, it is therefore possible to integrate this equation and obtain an estimate of ϕ_O over the entire $\boldsymbol{u}$-plane, out to the diffraction limit. A standard initial condition is to set $\phi_O(\boldsymbol{0}) = 0$, since the reconstructed image must be a real function, and therefore its transform must be Hermitian.

Bispectral Analysis. The standard way to calculate the image bispectrum (10) is to start from the triple correlation of a frame image, which is defined by

$$C(\boldsymbol{x}_1, \boldsymbol{x}_2) = \int I(\boldsymbol{x})I(\boldsymbol{x} + \boldsymbol{x}_1)I(\boldsymbol{x} + \boldsymbol{x}_2)\, d\boldsymbol{x} \tag{23}$$

The Fourier transform of the triple correlation is called the image bispectrum and can be written in the form

$$\hat{C}(\boldsymbol{u}_1, \boldsymbol{u}_2) = \hat{I}(\boldsymbol{u}_1)\hat{I}(\boldsymbol{u}_2)\hat{I}^*(\boldsymbol{u}_1 + \boldsymbol{u}_2) \tag{24}$$

Using Eq. (11), the right side of Eq. (24) may be rewritten in terms of the instantaneous point spread function and the true object intensity distribution, just as with the cross-spectrum. Averaging over many frames, this becomes

$$[\hat{C}(\boldsymbol{u}_1, \boldsymbol{u}_2)] = \hat{O}(\boldsymbol{u}_1)\hat{O}(\boldsymbol{u}_2)\hat{O}^*(\boldsymbol{u}_1 + \boldsymbol{u}_2)\langle \hat{S}(\boldsymbol{u}_1)\hat{S}(\boldsymbol{u}_2)\hat{S}^*(\boldsymbol{u}_1 + \boldsymbol{u}_2)\rangle \tag{25}$$

The quantity $\langle \hat{S}(\boldsymbol{u}_1)\hat{S}(\boldsymbol{u}_2)\ \hat{S}^*(\boldsymbol{u}_1 + \boldsymbol{u}_2)\rangle$ is known as the bispectral transfer function. It can be shown that the bispectral transfer function has zero phase, so that the phase of Eq. (25) is simply

$$\arg\{[\hat{C}(\boldsymbol{u}_1, \boldsymbol{u}_2)]\} = \arg[\hat{O}(\boldsymbol{u}_1)\hat{O}(\boldsymbol{u}_2)\hat{O}^*(\boldsymbol{u}_1 + \boldsymbol{u}_2)] \tag{26}$$

Consider the region of the bispectrum such that $\boldsymbol{u}_1 \equiv \boldsymbol{u}$ and $\boldsymbol{u}_2 \equiv \Delta\boldsymbol{u}$ with $\Delta\boldsymbol{u}$ some small fixed increment in frequency space. The bispectrum is a four-dimensional function for a two-dimensional image, so the requirement $\boldsymbol{u}_2 \equiv \Delta\boldsymbol{u}$ fixed defines a subplane of the bispectrum close to the plane $\boldsymbol{u}_2 = \boldsymbol{0}$. Let the phase of $\hat{O}$ at $\boldsymbol{u}$ be denoted by ϕ_0 as in the previous section and Eq. (26) may be rewritten as

$$\arg\{[\hat{C}(\boldsymbol{u}_1, \boldsymbol{u}_2)]\} = \phi_O(\boldsymbol{u}) + \phi_O(\Delta\boldsymbol{u}) - \phi_O(\boldsymbol{u} + \Delta\boldsymbol{u}) \tag{27}$$

If it were not for the term $\phi_0(\Delta\boldsymbol{u})$, this would again be a difference equation for the function $\phi_0(\boldsymbol{u})$ as with the cross-spectrum, and therefore an estimate of this function could be built up over the entire frequency plane using two nonparallel vectors $\Delta\boldsymbol{u}$ (or equivalently, using at least two subplanes from the bispectrum). The added term complicates this, but only slightly. If one chooses $\phi_0(\Delta\boldsymbol{u})$ arbitrarily, the effect on the recovered function $\phi_0(\boldsymbol{u})$ is to add a linear term to it. A linear phase term added to a function in frequency space merely translates the position of the inverse transform in image space, but image features are not affected. It is therefore sufficient to choose $\phi_0(\Delta\boldsymbol{u})$ arbitrarily for the purposes of image reconstruction. As with the Knox–Thompson algorithm, a standard initial condition to integrate the difference equation is to set $\phi_0(\boldsymbol{0}) = 0$.

Nakajima (11) gave the first general expression for the SNR of the bispectrum at arbitary light levels. At low light levels, the SNR is proportional to $n^{3/2}$, where n is the number of photons per frame. This can be compared to the power spectrum, where in the low light level regime, the SNR is proportional to n. In the low light regime, only the so-called "near axis" subplanes (subplanes with $\Delta\boldsymbol{u}$ small) have high SNR. For simple images, these subplanes are usually sufficient to derive good reconstructed images in the way discussed above. For more complicated images, other regions of the bispectrum may play a more important role in determining the phase map. Nakajima found that the limiting magnitude for bispectral analysis was between 13th and 15th magnitude, depending on telescope aperture size and seeing conditions.

Phase and Image Reconstruction. Bispectral analysis and the Knox–Thompson algorithm share the feature that they produce from the speckle data an estimate of the phase derivative of $\hat{O}(\boldsymbol{u})$ and this function must be integrated before it is combined with a modulus estimate obtained from the standard autocorrelation analysis of classical speckle interferometry. From this point there are two steps before arriving at a reconstructed image: (1) phase reconstruction and (2) Fourier inversion of $\hat{O}(\boldsymbol{u})$.

The phase is obtained from the bispectrum or cross-spectrum by integration, but it is possible to integrate the phase derivative map in several different ways, the simplest being via iteration, proposed by Lohmann et al. in 1983 (10). From the initial condition of zero phase at the origin (pixel 0) and the difference equation, the phase at pixel 1 is calculated, then from the value at pixel 1 and the difference equation, the value at pixel 2 is calculated, and so on. However, this method has the disadvantage that errors increase as the spatial frequency increase, making the phase estimate least reliable in the high-frequency region of frequency space. Another technique, used by Meng et al. (12), is a relaxation method, where zero phase or some initial guess at the phase map is assumed at the start and the phase at a particular pixel in the frequency plane is assigned by using the difference equation and the starting values of the phase at nearby pixels. This produces a new phase map, which replaces the initial guess and the process is repeated. After many iterations, the phases converge to the "correct" values. Still another method is to assume that the object has a particular intensity distribution (for example, assume that it is a binary star), and to do a best fit to the bispectrum (or cross-spectrum) to arrive at the correct phase map (13).

After the phase map is obtained and combined with the modulus estimate of an object, there is the matter of Fourier inversion to arrive at a reconstructed image. Essentially the problem is that to reconstruct the image unambiguously, one must know all of the Fourier components of the object, whereas in any real observation, only some of the components are obtained, and these all have some noise associated with them. Many techniques for Fourier inversion used so far in speckle imaging have been borrowed from radio astronomy. One example is the maximum entropy technique (14), which produces the smoothest map consistent with the data. Another approach is the "clean" algorithm (15), which assumes that the solution is a collection of point sources, and derives a map of their locations.

Observing Stellar Speckle Patterns

Several properties of stellar speckle patterns as observed through the atmosphere impose special requirements on the detection system. First, although a monochromatic speckle pattern was previously discussed and shown in Fig. 5, light from stars is not monochromatic. The character of speckle patterns is dependent on wavelength, in part because of a wavelength-dependent magnification of the image, and in part because of true differences in the optical path through the atmosphere as a function of wavelength. To avoid these problems, it is necessary to use a narrow-band pass filter to maintain a high degree of contrast to the patterns on the image plane. Using a narrow filter significantly reduces the total amount of light in of the speckle pattern, and limits the range of magnitudes for which the method is useful. In fact, the larger the telescope diameter, the narrower the band pass one must use, so that the limiting magnitude is only a weak function of collection area of the primary mirror of the telescope.

Another problem is that even with narrow-band pass filters, the color dispersion of the atmosphere (which is a function of zenith angle) is large enough to elongate speckles on

the image plane, and this effect must be removed. This is generally done with the use of two zero-deviation Risley prisms that can be rotated independently. The dispersions of the two prisms add vectorially, so it is possible to rotate the prisms to positions such that the resultant vector exactly counteracts the dispersion vector of the atmosphere in the direction of the target.

The techniques discussed above for deriving high-resolution information from stellar speckle patterns depend on the convolution relation, that is, that the frame image is the convolution of the frame speckle pattern and the true object intensity distribution. However, this assumes that the optical path through the atmosphere is identical for all points in the field of view of the telescope. For points very close together on the sky, this is a very good approximation, but as the separation between two points increases, their optical path through the atmosphere begins to diverge, and as they encounter different turbulent cells in the atmosphere, they generate different speckle patterns. This means that the deconvolution is only valid when all points of interest are contained within the region of the sky known as the "isoplanatic patch." The isoplanatic patch describes the area of sky over which speckle patterns remain very much the same and is usually only a few arcseconds in diameter at visible wavelengths, and perhaps 30 arcseconds in the near infrared.

Unlike laser speckle interferometry, where the speckle patterns can be controlled somewhat in the laboratory, a stellar speckle interferometer must have an imaging detector with several special characteristics. Most importantly, the imaging device must be capable of reading frames out at the rate of the evolution of the speckles; a minimum requirement is about 10 ms in the visible, and somewhat longer in the infrared. The detector must have relatively high quantum efficiency so that speckles in a single frame have sufficient contrast. Low read noise and low dark current are important because the number of detected photons per frame is usually small by astronomical standards. Since the goal is to obtain very high-resolution information inside a comparatively large seeing disk, excellent geometric fidelity and fairly large formats are necessary.

ELECTRONIC IMAGING DEVICES USED IN SPECKLE INTERFEROMETRY

In both laser and stellar speckle interferometry, TV cameras and photography were popular methods for recording speckle patterns in the 1970s, but in the 1980s and 1990s virtually all speckle pattern interferometry has been done with more sophisticated electronic imaging detectors. Current instrumentation can be divided roughly into two main categories: (1) photon-counting cameras (including intensified-CCDs), and (2) solid state detectors (i.e., CCDs and infrared arrays).

Photon-Counting Devices

Photon-counting imaging devices are cameras which make use of the photoelectric effect in such a way that they can detect individual photons. Several types of photon counters have been used for speckle imaging, including precision analog photon address (PAPA) detectors (16), resistive anode devices (13), wedge-and-strip detectors (17), multianode microchannel array (MAMA) detectors (18), and intensified-CCDs (19). By far the most popular of these is the intensified-CCD, but all use a microchannel plate (MCP) or MCP stack for signal amplification where the front end of the plate has a photocathode held at high voltage and the back end is held nominally at ground. A photon then strikes the photocathode and liberates one or more photoelectrons. As a photoelectron is accelerated through a microchannel, it contacts the channel wall several times and with each contact, secondary electrons are liberated. When the event exits the MCP, a total charge cloud of 10^5 to 10^7 electrons from a single input event can be produced. A microchannel therefore acts as a small, continuous photomultiplier tube when a photoelectron is accelerated through it. Figure 7 shows common types of high-gain MCPs. The photocathode can be made of a number of different materials, depending on what wavelength response is desired. Visible light photocathodes with reasonable quantum effiiency have been available for many years, and the one used with most photon-counting speckle interferometers is the so-called "S-20" or trialkali photocathode. The S-20 gives a quantum efficiency of about 10% through the visible and out to the near infrared.

Photon-counting devices have traditionally been used at low light levels, where CCDs cannot be used because of read noise. Because the same photocathode materials are available for all of these cameras, they all have about the same limiting quantum efficiency. The distinguishing feature separating one photon-counting camera from another is the way that the output of the MCP is detected. This process affects not only the overall quantum efficiency of the device, but also its linearity and timing resolution.

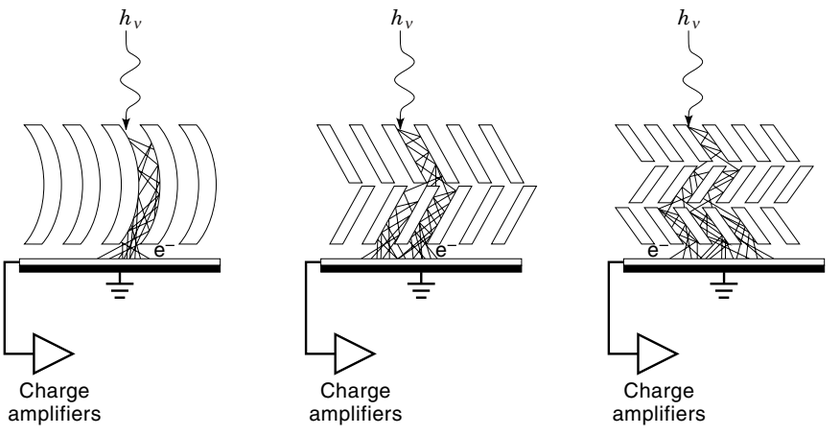

Figure 7. Three types of microchannel plate arrangements common in photon-counting detectors. The left-most example is a single curved channel MCP or C-plate, the middle example is known as a chevron arrangement, and the right-most example is known as a Z-stack. Copyright 1992 by D. B. Kasle, reprinted with permission.

Solid-State Detectors

CCDs. CCDs are an obvious choice for speckle work today because of the large formats that are available, their outstanding imaging characteristics, and their ease of use, especially in conjunction with computers. They are probably the most common devices for laser speckle intererometry, and indeed they are attractive for astronomical speckle interferometry because of their much higher quantum efficiency than the currently available photon-counting devices. Traditionally, they have had two drawbacks for stellar speckle interferometry. First, CCD readout speed has not been fast enough to take advantage of their quantum efficiency. Typically, the desired frame integration time is obtained by some sort of shuttering operation, then the frame is read out and meanwhile the detector is effectively "off," creating a large source of dead time. Second, their read noise also negates some of the advantage of the higher quantum efficiency by making it impossible for frames to have photon-limited statistics. This is especially important if the objects of interest are faint. Nonetheless, the properties of CCDs are improving very rapidly. It is possible now to obtain CCDs that can read out one million pixels per second with root-mean-square (rms) read noise of less than 10 electrons, and that have quantum efficiency of about 90% at 700 nm (7000 Å). For a 128 $\times$ 128 pixel subarray, this means that the device is capable of recording about 60 frames per second. The problems of read time and read noise do not affect laser speckle interferometry applications, since the light source and sample can be controlled in the laboratory.

Infrared Arrays. Infrared array technology has become very important for astronomy in the last decade. In the 1980s some one-dimensional arrays were used for speckle imaging, but more recently, some outstanding two-dimensional infrared speckle imaging has been possible with the advent of high-quality two-dimensional infrared arrays. InSb arrays have been used the most so far, which have a wavelength response from about 1 μm to 5 μm. A common format for the two-dimensional arrays used in the early 1990s in speckle imaging was 58 $\times$ 62 pixels, with larger arrays (256 $\times$ 256) available now. Like the CCDs discussed above, these arrays offer high quantum efficiency (about 80%), but read out the data in full frames. Today, the frame rates possible tend to be of order 10 per second (20), so as with visible CCDs, some of the advantage of the high quantum efficiency is sacrificed due to the detector dead time while frames are being read out.

SPECKLE INTERFEROMETRY TODAY

Astronomical Impact

In making scientific conclusions from high-resolution images reconstructed from speckle interferometry data, a primary concern is the quality of the reconstruction. This can be judged in terms of the fidelity of the astrometry of the image (measuring the relative positions of objects) and the photometry of the image (measuring the relative brightness of objects). While there is ample evidence that speckle interferometry can give astrometric results of outstanding quality (from the study of binary star orbits, for example), the photometric accuracy of the method is not on such firm ground. A recent paper by the leading group in binary star speckle interferometry states that it is difficult to determine the magnitude difference (or equivalently, the relative brightness) of the two stars in a binary system to better than 0.5 magnitudes, because of calibration problems and other issues (21). Since this is not very precise, and since a binary star system represents the simplest nontrivial photometric problem, this creates doubt about the photometric information of more complicated reconstructed images. Indeed, reconstructed images are generally assumed to have excellent astrometric information and imperfect photometric information. The problem of doing precise photometry with the speckle technique remains predominant in the field at the moment.

One of the most important aspects of speckle interferometry is that is has dramatically increased the awareness that many astronomers have about the power of optical interferometry and atmospheric compensation. This would not have been possible without some of the new instrumentation developed in the 1970s and 1980s, which has made speckle data taking more efficient and the observations themselves better. Now it is almost commonplace to measure objects in the sky with high angular resolution. In this sense, speckle interferometry has helped to pave the way for other kinds of high resolution astronomy such as adaptive optics and optical long-baseline interferometry, which are being pursued today.

Impact on Precise Measurement

Laser speckle interferometry provides a relatively easy way to make precise measurements, where in many cases the test object does not need to be prepared in any special way. This has brought the power and precision of interferometry to the fingertips of many engineers, but in addition, the use of electronic imaging has made the interpretation and manipulation of speckle data much easier. Though still limited in some ways, electronic speckle pattern interferometry offers the advantage of simplicity over holographic interferometry or speckle photography. With the advent of digital imaging devices, the number of analysis tools for use with speckle patterns has greatly increased, and continues to increase today, making electronic speckle pattern interferometry useful for a wider and wider range of measurement problems.

BIBLIOGRAPHY

1. E. Archibold, J. M. Burch, and A. E. Ennos, Recording of in-plane surface displacement by double-exposure speckle photography, *Opt. Acta,* **17**: 883–898, 1970.
2. G. Slettemoen, First-order statistics of displayed speckle patterns in electronic speckle pattern interferometry, *J. Opt. Soc. Am.,* **71**: 474–482, 1981.
3. J. A. Leendertz, Interferometric displacement measurement on scattering surfaces utilizing speckle effect, *J. Phys. E,* **6**: 214–218, 1970.
4. D. J. Schroeder, *Astronomical Optics,* San Diego: Academic Press, 1987.
5. A. Labeyrie, Attainment of diffraction limited resolution in large telescopes by Fourier analysing speckle patterns in star images, *Astron. Astrophys.,* **6**: 85–87, 1970.
6. W. G. Bagnuolo et al., Absolute quadrant determinations from speckle interferometry of binary stars, *Astron. J.,* **103**: 1399–1407, 1992.
7. R. H. T. Bates and F. M. Cody, Towards true imaging by wideband speckle interferometry, *Opt. Commun.,* **32**: 365–369, 1980.

8. S. P. Worden, C. R. Lynds, and J. W. Harvey, Reconstructed images of alpha Orionis using stellar speckle interferometry, *J. Opt. Soc. Am.,* **66**: 1243–1246, 1976.
9. K. T. Knox and B. J. Thompson, Recovery of images from atmospherically degraded short-exposure images, *Astrophys. J.,* **193**: L45–L48, 1974.
10. A. W. Lohmann, G. P. Weigelt, and B. Wirnitzer, Speckle masking in astronomy: Triple correlation theory and application, *Appl. Opt.,* **22**: 4028–4037, 1983.
11. T. Nakajima, Signal-to-noise ratio of the bispectral analysis of speckle interferometry, *J. Opt. Soc. Am. A,* **5**: 1477–1491, 1988.
12. J. Meng et al., Triple correlation subplane reconstruction of photon-address stellar images, *J. Opt. Soc. Am. A,* **7**: 1243–1250, 1990.
13. T. Nakajima et al., Diffraction-limited imaging. II. Optical aperture-synthesis of two binary stars, *Astron. J.,* **97**: 1510–1521, 1989.
14. J. Skilling and R. K. Bryan, Maximum entropy image reconstruction: General algorithm, *Mon. Not. R. Astron. Soc.,* **211**: 111–124, 1984.
15. P. W. Gorham et al., Recovery of diffraction-limited object autocorrelations from astronomical speckle interferograms using the CLEAN algorithm, *Astron. J.,* **100**: 294–306, 1990.
16. C. Papaliolios, P. Nisenson, and S. Ebstein, Speckle imaging with the PAPA detector, *Appl. Opt.,* **24**: 287–292, 1985.
17. J. Barnstedt, R. Neri, and M. Grewing, The AIT-MCP-detector system: Spectroscopic and speckle tests, *Mitt. Astron. Ges.,* **68**: 240–243, 1987.
18. J. S. Morgan, Speckle imaging with the MAMA detector, in F. Merkle (ed.), *High Resolution Imaging by Interferometry,* Garching bei München: European Southern Observatory, 1989.
19. H. A. McAlister et al., ICCD speckle observations of binary stars. II. Measurements during 1982–1985 from the Kitt Peak 4-m telescope, *Astron. J.,* **93**: 688–723, 1987.
20. D. W. McCarthy, Jr. et al., The low-mass companion of Gliese 22A: First results of the Steward Observatory infrared speckle camera, *Astron. J.,* **101**: 214–219, 1991.
21. W. I. Hartkopf et al., ICCD speckle observations of binary stars. XIII. Measurements during 1989–1994 from the Cerro Tololo 4-m telescope, *Astron. J.,* **111**: 936–945, 1996.

Reading List

J. C. Dainty (ed.), *Laser Speckle and Related Phenomena,* Munich: Springer-Verlag, 1984.

J. W. Goodman, *Statistical Optics,* New York: Wiley, 1985.

M. C. Roggemann and B. Welsh, *Imaging through Turbulence,* Boca Raton, FL: CRC Press, 1996.

ELLIOTT HORCH
Rochester Institute of Technology

ELECTRONICS, SUPERCONDUCTING. See SUPERCONDUCTING MICROWAVE TECHNOLOGY.

ELECTRONICS, THERMAL. See THERMAL ANALYSIS AND DESIGN OF ELECTRONIC SYSTEMS.

ELECTRONIC TRANSPORT, HIGH FIELDS. See HIGH-FIELD EFFECTS.